The cosmic infrared background experiment-2 (CIBER-2) for studying the near-infrared extragalactic background light

Mai Shirahata[a], Toshiaki Arai[a,b], John Battle[c], James Bock[c,d], Asantha Cooray[e], Akito Enokuchi[f], Viktor Hristov[c], Yoshikazu Kanai[f], Min Gyu Kim[g], Phillip Korngut[c,d], Alicia Lanz[c], Dae-Hee Lee[g], Peter Mason[c], Toshio Matsumoto[a,h], Shuji Matsuura[i,a], Tracy Morford[c], Yosuke Ohnishi[j], Won-Kee Park[g], Kei Sano[k], Norihide Takeyama[f], Kohji Tsumura[b], Takehiko Wada[a], Shiang-Yu Wang[h], and Michael Zemcov[l,d]

[a]Institute of Space and Astronautical Science (ISAS), Japan Aerospace Exploration Agency (JAXA), Sagamihara, Kanagawa 252-5210, Japan;
[b]Frontier Research Institute for Interdisciplinary Science, Tohoku University, Sendai, Miyagi 980-8578, Japan;
[c]Department of Physics, Mathematics and Astronomy, California Institute of Technology, Pasadena, CA91125, USA;
[d]Jet Propulsion Laboratory (JPL), National Aeronautics and Space Administration (NASA), Pasadena, CA91109, USA;
[e]Center for Cosmology, University of California, Irvine, CA 92697, USA;
[f]Genesia Corporation, Mitaka, Tokyo 181-0013, Japan;
[g]Korea Astronomy and Space Science Institute (KASI), Yuseong-gu, Daejeon 305-348, Republic of Korea;
[h]Institute of Astronomy and Astrophysics, Academia Sinica, Taipei 10617, Taiwan, R. O. C.;
[i]School of Science and Technology, Kwansei Gakuin University, Sanda, Hyogo 669-1337, Japan;
[j]Department of Physics, Tokyo Institute of Technology, Meguro, Tokyo 152-8551, Japan;
[k]Graduate School of Science, University of Tokyo, Bunkyo, Tokyo 113-0033, Japan;
[l]School of Physics and Astronomy, Rochester Institute of Technology, Rochester, NY 14623-5603, USA

ABSTRACT

We present the current status of the Cosmic Infrared Background ExpeRiment-2 (CIBER-2) project, whose goal is to make a rocket-borne measurement of the near-infrared Extragalactic Background Light (EBL), under a collaboration with U.S.A., Japan, South Korea, and Taiwan. The EBL is the integrated light of all extragalactic sources of emission back to the early Universe. At near-infrared wavelengths, measurement of the EBL is a promising way to detect the diffuse light from the first collapsed structures at redshift $z\sim10$, which are impossible to detect as individual sources. However, recently, the intra-halo light (IHL) model is advocated as the main contribution to the EBL, and our new result of the EBL fluctuation from CIBER-1 experiment is also supporting this model. In this model, EBL is contributed by accumulated light from stars in the dark halo regions of low-redshift ($z<2$) galaxies, those were tidally stripped by the interaction of satellite dwarf galaxies. Thus, in order to understand the origin of the EBL, both the spatial fluctuation observations with multiple wavelength bands and the absolute spectroscopic observations for the EBL are highly required. After the successful initial CIBER-1 experiment, we are now developing a new instrument CIBER-2, which is comprised of a 28.5-cm aluminum telescope and three broad-band, wide-field imaging cameras. The three wide-field (2.3×2.3 degrees) imaging cameras use the $2K\times2K$ HgCdTe HAWAII-2RG arrays, and cover the optical and near-infrared wavelength

Further author information: (Send correspondence to Mai Shirahata)
Mai Shirahata: E-mail: mai@genesia.co.jp, Telephone: +81 (422) 76-2773, Fax: +81 (422) 76-2774, Genesia Corporation, Mitaka Sangyo Plaza 601, 3-38-4 Shimorenjyaku, Mitaka Tokyo 181-0013, Japan

Space Telescopes and Instrumentation 2016: Optical, Infrared, and Millimeter Wave, edited by Howard A. MacEwen, Giovanni G. Fazio, Makenzie Lystrup, Proc. of SPIE Vol. 9904, 99044J · © 2016 SPIE · CCC code: 0277-786X/16/$18 · doi: 10.1117/12.2229567

range of 0.5–0.9 μm, 1.0–1.4 μm and 1.5–2.0 μm, respectively. Combining a large area telescope with the high sensitivity detectors, CIBER-2 will be able to measure the spatial fluctuations in the EBL at much fainter levels than those detected in previous CIBER-1 experiment. Additionally, we will use a linear variable filter installed just above the detectors so that a measurement of the absolute spectrum of the EBL is also possible. In this paper, the scientific motivation and the expected performance for CIBER-2 will be presented. The detailed designs of the telescope and imaging cameras will also be discussed, including the designs of the mechanical, cryogenic, and electrical systems.

Keywords: CIBER-2, near-infrared background, rocket, observation, telescope

1. INTRODUCTION

CIBER-2 (the Cosmic Infrared Background ExpeRiment-2) is a sounding rocket experiment project aimed to measure spatial fluctuations in the near-infrared background light. CIBER-2 scientifically follows on the detection of fluctuations with the predecessor CIBER-1 sounding rocket experiment,[1–4] and will use measurement techniques developed and successfully demonstrated by CIBER-1,[5] Thanks to the high-sensitivity and multi-band imaging measurements, CIBER-2 will elucidate the history of Intra-halo light (IHL) production[6] and carry out a deep search for extragalactic background fluctuations associated with the epoch of reionization (EOR).[7,8]

CIBER-1 has made high-quality detections of large-scale fluctuations of EBL over 4 flights.[1,5] CIBER-1 measured the amplitude of fluctuations on arcminute scales, 1.7 and 1.5 nWm^{-2}sr^{-1} at 1.0 and 1.6 μm, respectively. The electromagnetic spectrum of the fluctuations, detected in both auto- and cross-correlations with 3.6 μm Spitzer data, is close to Rayleigh-Jeans spectrum, but with a statistically significant turnover at 1.1 μm. This spectrum is significantly bluer than that of the integrated galactic light (IGL) derived from galaxy counts.[6,9,10] We interpret the CIBER-1 fluctuations is arising from IHL, low-mass stars tidally stripped from their parent galaxies during galaxy mergers at a redshift of $0<z<2$. The first generation of stars and their remnants are likely responsible for the reionization of the intergalactic medium, observed to be ionized out to the most distant quasars at a redshift of $z\sim6$. The total luminosity produced by first stars is uncertain, but a lower limit can be placed assuming a minimal number of photons to produce and sustain reionization.[11] This minimal extragalactic background component associated with reionization is detectable in fluctuations at the design sensitivity of CIBER-2.[12]

CIBER-2 is optimized to have sufficient sensitivity to probe the faint signal level of EBL, even in a short observation time of the sounding rocket flight. The expected depth of CIBER-2 fluctuation measurements, comparing with the previous measurements of CIBER-1,[5] AKARI,[13] and Spitzer,[14,15] are shown in Figure 1. CIBER-2 will determine the origin and history of EBL fluctuations by carrying out multi-wavelength imaging in 6 spectral bands ranging from 0.5 to 2.0 μm. CIBER-2 will extend the CIBER-1 observations from the near-infrared into the optical. Observations at optical wavelengths are key, because optical EOR emission will be strongly absorbed due to Lyman absorption at $z\sim7$, while IHL emission from old low-mass stars will have a peak near 1.5 μm and slowly decrease. Therefore, we will be able to distinguish the EOR and IHL components by its optical spectrum. We will study the history of IHL production by implementing a multi-band cross-correlation analysis, and use this information to carry out a deep search for an EOR component. In subsequent flights we plan joint observations with weak lensing maps, with an optimized set of filter bands to measure spectral cross-correlations, to fully elucidate the history of IHL light production.

In this paper we describe the current status for the development of CIBER-2. CIBER-2 consists of a Cassegrain telescope assembly, imaging optics, and cryogenic mounted aboard a sounding rocket. The aspect of the CIBER-2 is shown in Figure 2. From the next section we describe the detail.

2. SOUNDING ROCKET AND CRYOGENICS

CIBER-2 will be launched under the NASA sounding rocket program with the Black Brant IV.[19] The outer diameter of the rocket skin is 438.4 mm and the length of a payload part is 1231.0 mm. The instrument must be fit in this space. The telescope assembly and imaging optics are housed in an evacuated segment of the payload, and are cooled to the temperature of $\sim$80 K by an on-board liquid nitrogen reservoir. This payload part is capped at the aft end of the rocket, toward the motors, by a door that opens to the telescope aperture.

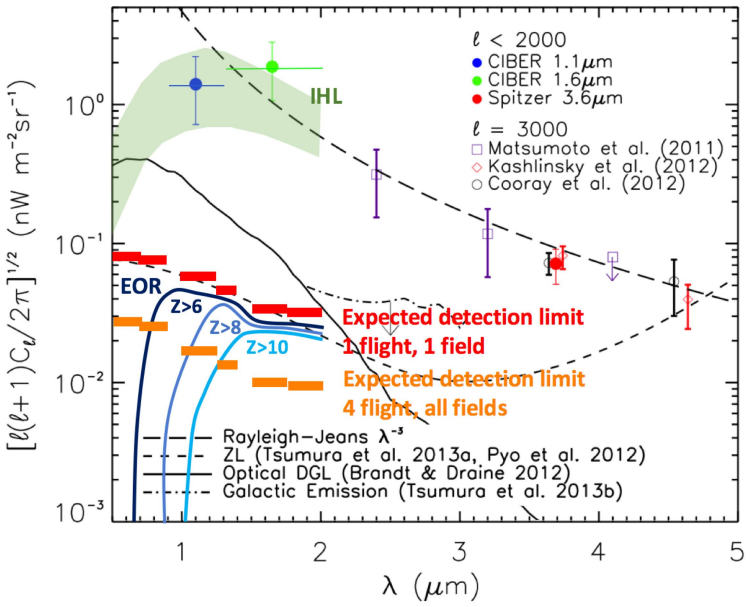

Figure 1. The depth of CIBER-2 fluctuation measurements in 6 bands from 0.5–2.0 μm at a particular angular scale. The red lines indicate the depth achieved by CIBER-2 in a single flight using one field. The orange lines indicate the depth from all data in four flights. The green band indicates the predicted level of IHL across the wavelength range.[5] The three lines show the expected contribution to EBL fluctuations from early galaxies assuming different reionization histories (EOR), with the dark blue line (left) for z>6, blue line (middle) for z>8, and light blue line (right) for z>10. The blue and green circles shows the results of the fluctuation measurements of the fluctuation power from CIBER-1.[5] Also indicated at wavelength larger than 2 μm are previous measurements from AKARI[13,16–18] and Spitzer.[14,15]

The CIBER-2 cryogenic system is a duplicate of the successful cryogenic system used in CIBER-1. This system consists of a 7 liter liquid nitrogen vessel filled with an open-cell aluminum foam that ensures thermal contact between liquid and metal in zero-gravity conditions. The optical bench supporting the imaging optics are mounted directly to the cryostat. G-10 plates mount the cryostat to the thermal vacuum bulkhead that marks the forward boundary of the vacuum payload. This bulkhead has hermetic connections for cabling to travel from the vacuum payload part to the warm electronics part, where the electronics are located.

The telescope assembly, imaging optics, and cryogenic system are enclosed in a radiation shield made of Aluminum 1100, mounted to the cryostat for cooling. The radiation shield buffers the cryogenically cooled instruments from radiation from the skin. The radiation shield is wrapped in a Mylar blanket to further reduce the radiative load. A pop-up baffle provides additional shielding from stray light from the rocket skin and shutter door. This pop-up baffle is stowed inside the telescope assembly upon ascent and descent, and deployed to extend beyond the lip of the skin during observations. The shutter door has additional blackened baffling covers that are stood off from the door itself with Vespel posts.

3. TELESCOPE ASSEMBLY

3.1 Design of the telescope assembly

CIBER-2 employs a Ritchey-Chretien type telescope. The entrance pupil diameter at the primary mirror is 285 mm, and the diameter of the secondary mirror is 105 mm. The F number of the telescope assembly is F/3.26 overall. All telescope assembly, including the primary and secondary mirrors, are made by Aluminum, RSA6061-T6, in order to reduce the thermal stress with the rocket skin made by Aluminum. The specifications of the CIBER-2 telescope assembly are summarized in Table 1.

The primary mirror is mounted to the base-plate via three Aluminum (A6061-T6) flexures. These flexures are required to relieve the mechanical stress to the mirror surface when installing the primary mirror. The secondary

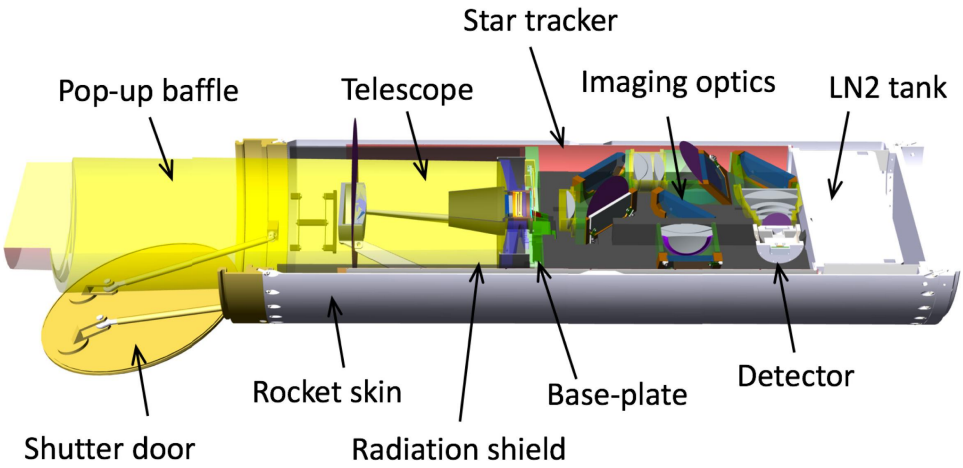

Figure 2. The aspect view of the CIBER-2. A 28.5 cm Cassegrain telescope reflects light to the imaging optics, where two beam splitters separate the light into three optical paths. Each optical path travels to one of the three focal plane assemblies. Each focal plane has a dual window pane filter, providing two spectral bands per single detector array, and six bands in total at 0.5–2.0 μm. The detector array is the 2K×2K HgCdTe HAWAII-2RG array. In addition, each focal plane incorporates a linear variable filter covering a small area of the array. Additional cold star tracker is placed next to the imaging optics in order to improve the attitude stability. A liquid nitrogen cryostat, copies from CIBER-1 instrument, cools the telescope, optics, and detectors to a temperature of ∼80 K. A cryogenic pop-up baffle that extends during observations and radiatively-coold door are used to reduce thermal emission from the rocket skin from scattering into the optics. Warm readout electronics and a warm star tracker are mounted to the forward end of the part on a vacuum bulkhead.

Table 1. Specification of the CIBER-2 telescope.

Telescope type	Ritchey-Chretien
EPD (Entrance Pupil Diameter)	285 mm (at primary mirror)
EFL (Equivalent Focal Length)	930 mm
Arm-S	930.86 mm
Arm-M	929.61 mm
Arm-L	930.02 mm
FNO (F Number)	3.26
Arm-S	3.266
Arm-M	3.262
Arm-L	3.263
FOV (Field of View)	2.3×2.3 degree^2
Detector Format	2048×2048 pixels (Pixel size = 18 μm)
Pixel Scale	4 arcsec / pixel

mirror is held up by four support spiders that mount to the base-plate. The number of support spiders, four, has been decided by the requirements that the PSF shape should be a symmetry for the EBL fluctuation analysis.

3.2 Technical improvement

The telescope assembly is designed and developed by Genesia Corporation of Japan. We have made a BBM (Bread Board Model) of the Aluminum telescope (see Figure 3), and measured the surface roughness and shape of the primary mirror attached with flexures by using the interferometer Zygo and CGH (Computer Generated Hologram). The measured surface roughness as the peak-to-peak value is approximately 1.0-lambda with HeNe

laser at 633 nm. We found a major distortion with 3-fold rotational symmetry caused by the stress from the mirror supports. For the FM (Flight Model) mirror we polish the mirror surface down to 0.5-lambda level in final manufacturing process.

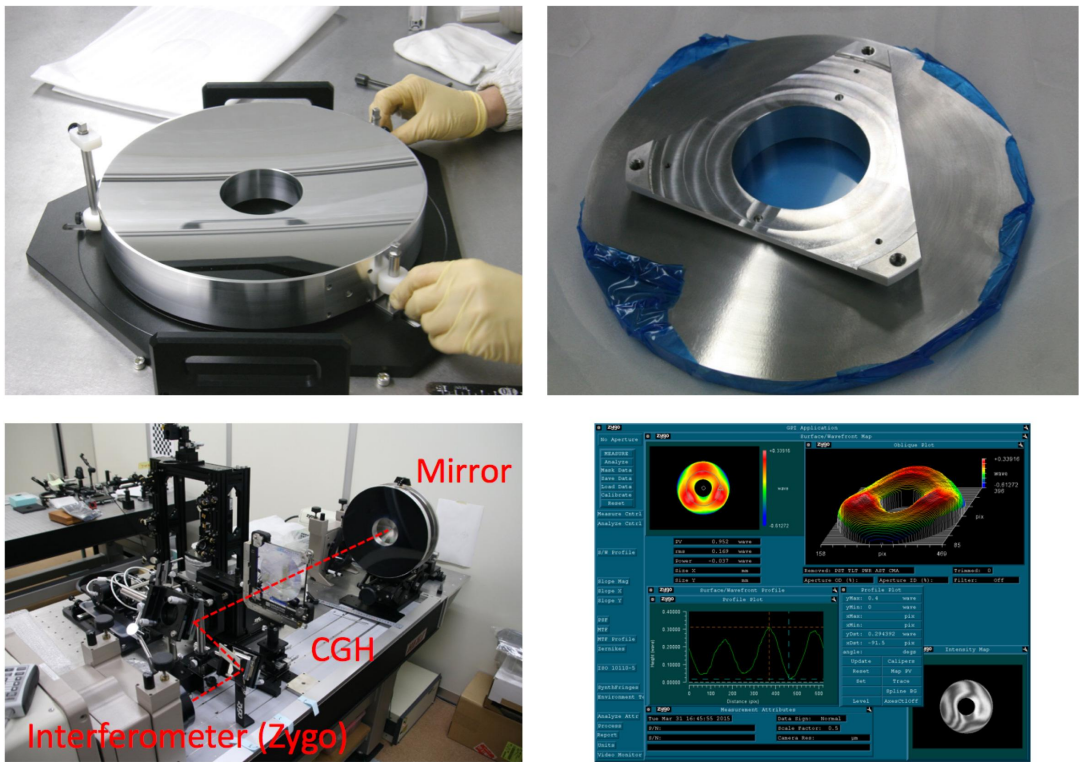

Figure 3. **(top left)** photograph of the BBM primary mirror surface. **(top right)** photograph of the BBM primary mirror backside. **(bottom left)** measurements system for the BBM primary mirror. **(bottom right)** the results of the Zygo interferometer measurements.

The surface roughness of Aluminum mirrors will be around 0.5-lambda for the FM mirrors. After grinding and polishing of the mirror surfaces, it will be coated with Ag and TiO_2 coating layers; This coating is effective not only to increase the reflectivity at the mirror surface in 0.5–2.0 μm (see Figure 4), but also to protect the mirror surface against scratching during handling and to allow easy cleaning. However, the coating layer should be thin so as not to give any stress to the mirror during cool down due to difference of CTE (coefficient of thermal expansion) between Ag and Al in cooling. We measured temperature dependence of the flatness of an Ag-coated flat mirror using a laser source and confirmed that the distortion at low temperature is within acceptable range.

3.3 contrived components

A cylindrical optical fixed baffle that provides both structural support and light shielding is also attached to the base-plate. Titanium flexures fix the optical baffle to a mounting ring that is attached directly to the rocket skin. These flexures relieve mechanical stress and provide a thermal break between the rocket skin and the cold telescope assembly. A radiatively cooled black cover will eliminate any stray emission from the door part, and a pop-up baffle will be deployed in flight to shield the optics from thermal radiation from the skin and environment.

A cold shutter implanted to the base-plate allows us to record dark frames prior to launch, and also in flight. A calibration source mounted behind the secondary mirror uses a combination of LEDs and a Halogen lamp to provide a known illumination in each spectral band, giving a transfer standard to compare before and during flight.

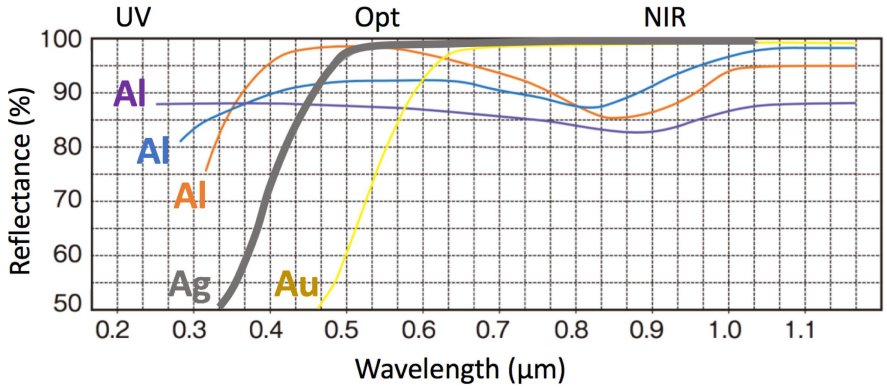

Figure 4. typical reflectance for metal coating. The wavelength range of CIBER-2 observation is 0.5–2.0 μm.

4. IMAGING OPTICS

4.1 Design of the imaging optics

The CIBER-2 imaging optics are designed to observe the EBL in the wavelength range of 0.5 to 2.0 μm. The three imaging optics have a wide Field of View, 2.3×2.3 degrees^2. Each imaging optics, called as Arm-S, Arm-M, and Arm-L, cover the optical and near-infrared wavelength range of 0.5–0.9 μm, 1.0–1.4 μm, and 1.5–2.0 μm, respectively, combining with the HgCdTe HAWAII-2RG arrays. Figure 5 shows an optics layout of CIBER-2.

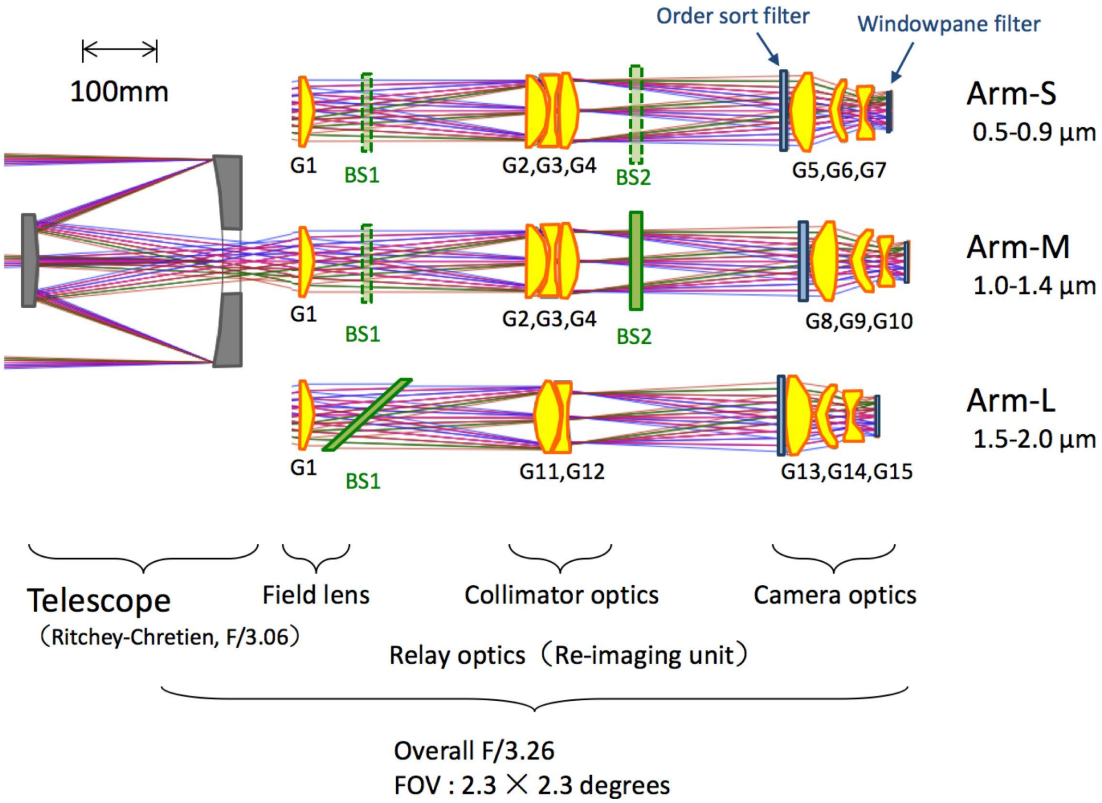

Figure 5. CIBER-2 imaging optics outline. Incoming light is split into three light paths using a field lens, collimator optics, camera optics, two dichroic beam splitters, band pass filters (order sort filter and windowpane filter) direct the light to a focal plane assembly that contains a detector array.

As shown in Figure 5, light from the telescope passes through the Cassegrain hole to the imaging optics part, where it is focused by a common field lens. Next, the first dichroic beam splitter (BS1) separates the incoming light at the wavelength of 1.45 μm into two paths, one is for the Arm-S and Arm-M, and the other is for the Arm-L. Then each light path goes through the collimator optics. As for the Arm-S and Arm-M path, the second dichroic beam splitter (BS2) separates the light at the wavelength of 0.95 μm into two paths. Finally, three light paths arrive at the imaging surface through the camera optics. The order sort filters in front of the camera optics define the band path wavelength for 3 arms, while the window pane filter just in front of the detector array splits the light into two wavelength bands within each arm. As a result, six observational wavelength bands in total span in the wavelength range of 0.5–2.0 μm, and the FOV for each band has 2.0×1.1 degrees^2. Figure 6 indicates the band definition for 6 bands. Because the cut-on/-off wavelength of the beam splitters have the large dependence on the angle of incidence, there are unused wavelength gaps between arms, 0.9–1.0 μm and 1.4–1.5 μm for Arm-S/-M and Arm-M/-L, respectively.

In addition to the 6 broad imaging bands, a small area of each focal plane will be imaged with a linear variable filter (LVF). The spectral resolution of the LVF measurements is $R=\lambda/\Delta\lambda\sim20$ and the FOV for the LVF measurements is 1.5×0.3 degrees^2. Figure 7 shows the photograph of the LVF filters and its transmittance at the room temperature. In order to measure the dark current for a reference, small areas of both LVF sides are covered with dark masks (See Figure 8). These LVF filters will be used for absolute spectro-photometric measurements of the EBL at wavelengths 0.5–2.0 μm. The CIBER-2 LVF measurements will be significantly more capable than the CIBER-1 LRS observations.[20,21] The higher spatial resolution in imaging mode allows us to accurately subtract stars individually, whereas the accuracy of the foreground star subtraction was limited in the CIBER-1 LRS observations based on a slit spectroscopy.

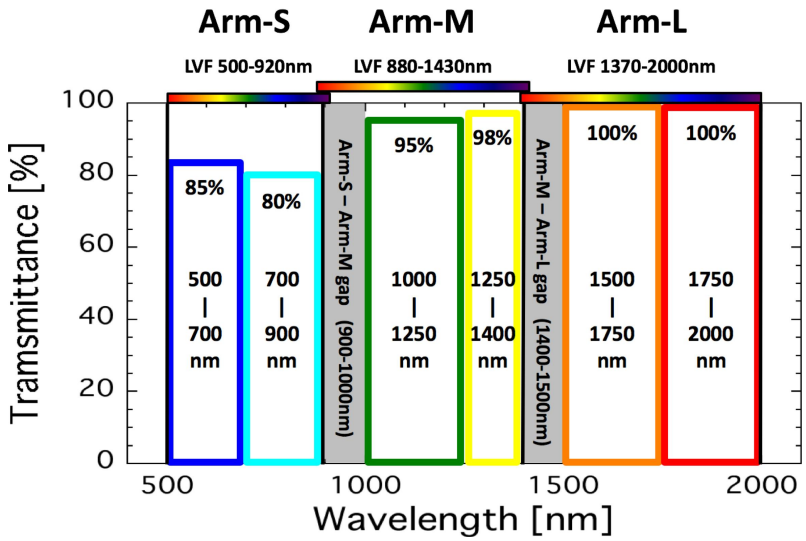

Figure 6. Band definition for CIBER-2.

4.2 Optical performance of the imaging optics

The optical design for CIBER-2 is made by Genesia Corporation of Japan. From the scientific point of view, two conflicting peculiarities are required for this imaging optics. One is the high light focusing power to take point sources off efficiently from the observational images. The other is mounting each module compactly in the limited space within the rocket skin. Hence, the CIBER-2 imaging optics adopt many aspheric lenses. This is very useful not only to reduce the number of lens elements but also to improve the light focusing property. As a result, they obtained the splendid design, in which more than 90 % encircled energy for point sources is collected in 3×3 pixels over the whole field of view for all 3 arms. The expected encircled energies for this optical design are shown in Figure 9.

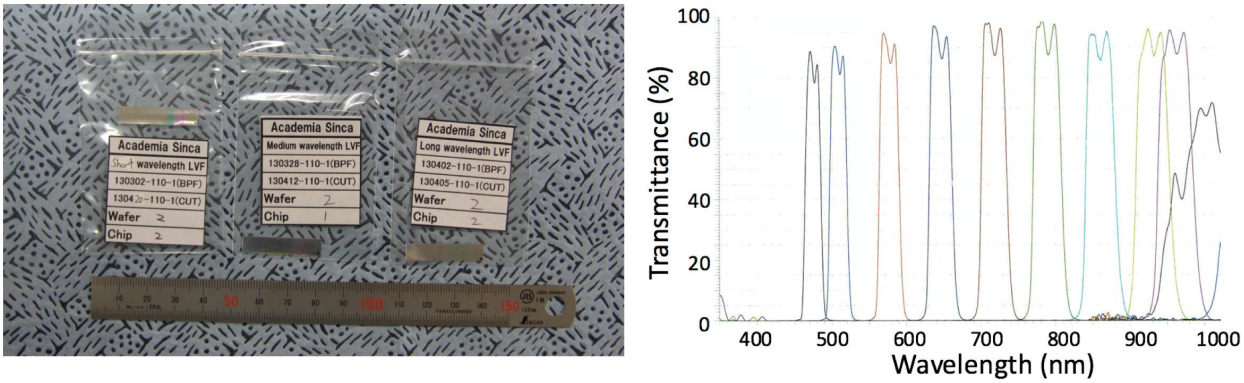

Figure 7. **(left)** LVF filters for three arms. **(right)** LVF filter transmission spectrum obtained for the Arm-S at the room temperature.

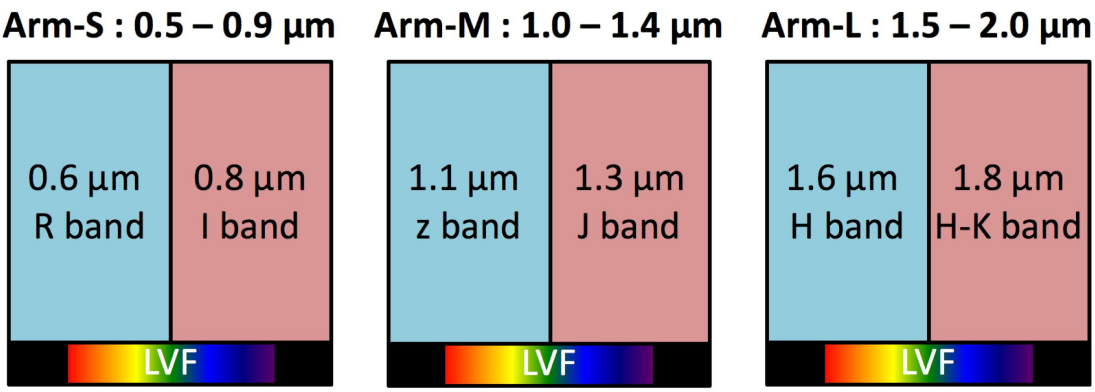

Figure 8. The layout of filters on the detector array.

4.3 Current status of the development

At the moment of this paper, all of 15 lenses have been polished. 12 aspheric lenses have been polished by Natsume Optical Corporation. The AR coating is going to be done by Optical Coatings Japan. Coating to the lenses with strong curvatures was a technology challenge, but our new development made this feasible.

All of the optical components are supported by flexures and retainers in the lens barrel to handle the thermal compression stress in cooling and to maintain optical alignment against vibration and shock during launch. The imaging optics are mounted to an optical bench that connects the base-plate and the cryogenic tank. All of the mechanical parts are designed by Genesia Corporation in Japan, and are machined at ASIAA in Taiwan.

5. FOCAL PLANE UNIT

Focal plane assemblies provide housing for the detector arrays, windowpane filters, LVF filters, and a circuit board for the first stage of detector readout, as shown in Figure 10. The detector arrays are thermally stood off from the optical assembly by a Molybdenum support structure, limiting the rate of temperature change below 2K/min during cooling and allowing for the inclusion of a thermal regulation feedback system to stabilize the focal plane temperature during flight. The thermal stabilization system consists of a heating resistor and thermometer mounted to the focal plane, with the amount of power dissipated by the heater controlled by a proportional-integral-derivative (PID) loop. A filter assembly is mounted to the Molybdenum support structure, suspending a set of windowpane filters and LVF filters just above the detector array. The detector array and

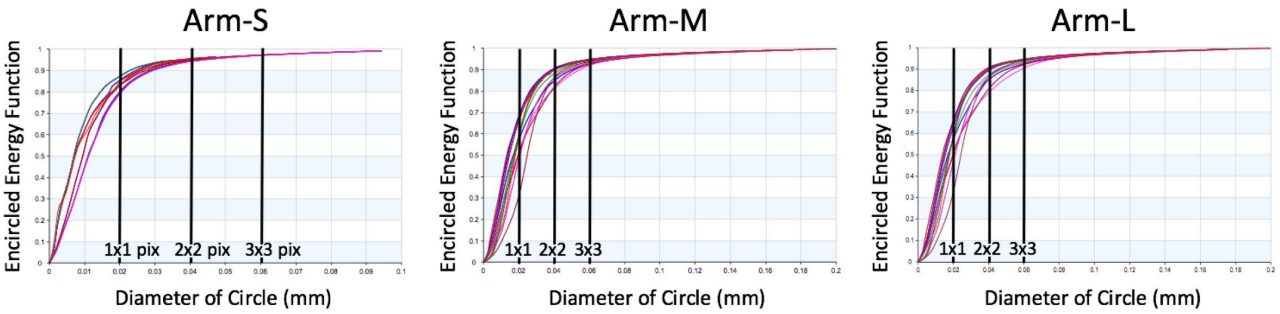

Figure 9. Encircled energy function for Arm-S, Arm-M, and Arm-L, respectively. The vertical lines with the label of X-pix indicate the diameter of circle which has the same area of X-pixels.

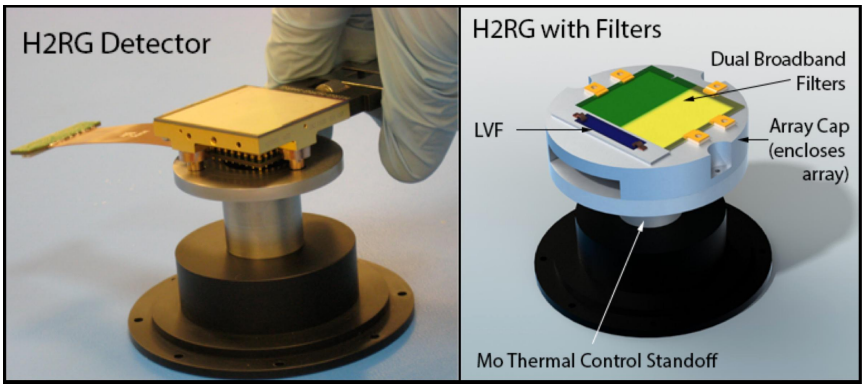

Figure 10. **(left)** HAWAII-2RG detector array undergoing installation onto a Molybdenum support structure. **(right)** model of filter assembly, with array cap supporting a windowpane filter and a LVF filter.

filter assembly are encased in an aluminum assembly. This assembly also houses a focal plane board for read out of the detector electronics.

6. DETECTOR AND ELECTRONICS

CIBER-2 employs three HAWAII-2RG (H2RG) detector arrays,[22,23] which are second-generation commercial HgCdTe near-IR detectors with a pixel format of 2048 × 2048 manufactured by Teledyne Scientific and Imaging Corporation. HAWAII-2RG detector arrays will use on-chip amplifier chopping which reduces the $1/f$ noise from the readout chain, reducing the need for complex Fourier weighting techniques employed with the CIBER-1 data. Each detector is biased and read out by custom electronics on the focal plane boards. The 2048 columns of the detector array are divided into 32 channels, which are read out in slow mode to reduce readout time and noise. Since the pixel voltages have a large offset, an external reference voltage close to the average pixel voltage is used to remove the offset. A reference pixel row will be read out periodically during the full detector array readout, providing a method of $1/f$ noise mitigation.[23]

The data rate required for three detectors exceeds the capabilities of the NASA ground telemetry systems. Instead of transmitting all data and housekeeping down to the ground station, CIBER-2 stores flight data on-board and transmits only a small fraction for diagnostic purposes. Solid-state storage is required to withstand the physical environment experienced in flight. Each detector array requires one data storage board with two 128 GB flash memory chips. This data storage board receives the digitized detector array output data from the array processing and housekeeping board and stores a primary and backup copy on each of the flash memory chips. Housekeeping data and a single channel of flight data are transmitted via rocket telemetry systems to the ground station. Raw rocket telemetry received by the ground system is forwarded to custom ground station

elections (GSE) which displays the data in real time. More details about the CIBER-2 electronics are described in Alicia et al. (2014).

7. COLD STAR TRACKER

The experimental module for CIBER-1 employed a star tracker (STT) located outside the cold science instrument part. In the CIBER-1 flight, we found the pointing drift during the observation by alignment change of the STT against the cold telescope due to aerodynamic heating in ascent. For CIBER-2, therefore, we adopt a cold STT placed at the focal plane of the telescope in addition to the warm STT same as CIBER-1.

The cold STT is also designed by Genesia Corporation. In order to make this STT optics compact, the primary and secondary mirrors are shared with the imaging optics, but STT uses only oblique incidence just out of the imaging optics field. The relay optics for the cold STT optics consists of three aspheric lenses and one spherical lens. The most important performance for the cold STT is providing the stable PSF with which a system can determine the center of the stellar coordinate. The cold STT optics compensate astigmatic aberration of Cassegrain telescope, and use spherical aberration to fill centered obscuration caused by secondary mirror. In addition, it has a spread PSF to make image flower for stable focus depth by producing spherical aberration. The wavelength coverage for the cold STT is 500–900 nm, which is determined to minimize chromatic aberration. The resultant encircled energy for the cold STT optics is shown in Figure 11.

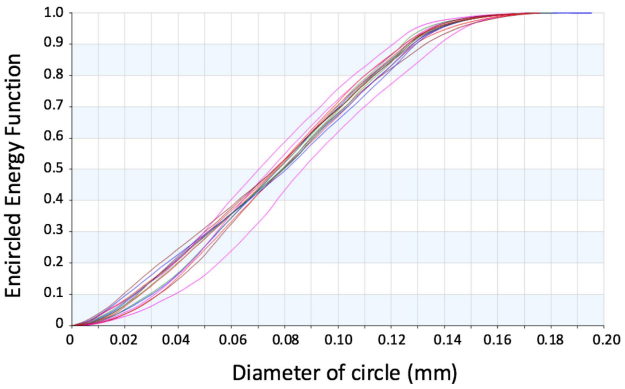

Figure 11. The encircled energy for the cold STT.

8. ROCKET PAYLOAD

The NASA Sounding Rocket Program is described in Reference 13. The Sounding Rocket program provides standardized systems for launch, payload separation, active pointing during flight, real time telemetry, and parachute recovery. CIBER-2 is designed to launch on the Black Brant IX vehicle system, consisting of a Mark 70 Terrier booster stage and a Black Brant sustainer. These motors make up the aft end of the rocket. Moving forward, the entire rocket consists of a payload separation system, the CIBER-2 instrument, the CIBER-2 warm electronics, a telemetry part, an active guidance system, an attitude control system, and finally the ogive recovery system.

The CIBER-2 launch sequence closely follows the launch sequence of CIBER-1 flights.[1] The Mark 70 Terrier rocket motor burns for approximately 6 seconds for launch. This segment has guide fins that cause the rocket to spin at a rate of approximately 4 Hz, providing thrust axis stability. Once burn is complete, the motor is separated from the rest of the rocket by drag. The second stage burns for approximately 30 seconds then is ejected from the remaining rocket parts by the payload separation part. Next, cables with weighted ends are released from the payload part to reduce the spin rate of the rocket to a rate of approximately 0.5 Hz. Once the lower spin rate is achieved, the cables are released. The telescope shutter door opens, and the pop-up baffle comes

out. Then observations begin. Upon completion of observations and prior to re-entry, the telescope shutter door is closed and the pop-up baffle is retracted in the rocket skin. The observation time with the altitude higher than 200 km is 400 seconds. Gas expelled from the attitude control system is used to increase the rocket spin rate to approximately 1 Hz. The rocket re-enters the atmosphere and the parachute deploys when the rocket reaches a height of 16,000 feet. The payload has a velocity of approximately 30 ft/s when it collides with the ground. Recovery of the payload begins several hours after completion of flight. Payload recovery is crucial for CIBER-2, as the data collected in flight will be stored on the rocket.

9. FLIGHT OBSERVATION

CIBER-2 plans two flights in the configuration described in this paper. The first flight is planned for 2018 with the second flight to follow six months later. The flights are separated by six months for consistency checks on absolute photometry measurements with the LVF spectrometer, as the Zodiacal foreground is modulated by the Earths annual path around the sun. Two flights will also allow for cross correlation between CIBER-2 flight data to characterize and eliminate instrumental artifacts. Additional flights are planned with different optical configurations, such as modified wavebands.

CIBER-2 observes five fields during a flight.[20] These fields are chosen to coincide with previous optical and spatial fluctuation observations[6,9,10] for cross correlation and point source removal. Additionally, launch windows are defined so that the sun and moon are below the depressed horizon. Typical candidate fields are Bootes, North Ecliptic Pole, Lockman Hole, and ELAIS-N1. CIBER-2 observes each field for 35 seconds at two different roll angles to center each of the wavelength bands on the same sky. Each field thus has a total observation time of 70 seconds per field.

CIBER-2 data is processed by a custom data analysis pipeline.[2,5] Raw data retrieved from the rocket payload is a time stream that must be converted into detector array images, calibrated, flat-field corrected, and aligned on the sky. Bright astronomical sources (J-band $\sim$ 19 AB magnitude) are masked, as are any residual source structure, such as diffraction spikes due to CIBER-2 secondary mirror support structures. The power spectrum of a sky image is then generated. Contributions to the power spectrum from instrumental and photon noise, the beam transfer function, and the effects of mode coupling due to masking of sources are then modeled and quantified. As CIBER-2 observes in six spectral bands, a total of 21 auto- and cross-spectra are available for science analysis. Various contributions to the large scale EBL fluctuations will be identified from spectral decomposition of the auto- and cross-spectra.

ACKNOWLEDGMENTS

This work was supported by NASA APRA research grants NNX07AI54G, NNG05WC18G, NNX07AG43G, NNX07AJ24G, and NNX10AE12G. Japanese participation in CIBER was supported by KAKENHI (21111004, 15H05744, 26800112) from Japan Society for the Promotion of Science (JSPS) and the Ministry of Education, Culture, Sports, Science and Technology (MEXT). Korean participation in CIBER was supported by the Pioneer Project from Korea Astronomy and Space Science Institute (KASI). P.K. acknowledge support from NASA Postdoctoral Program Fellowships, A.C. acknowledges support from an NSF CAREER award AST-0645427 and NSF AST-1313319.

REFERENCES

[1] Zemcov, M., Arai, T., Battle, J., Bock, J., Cooray, A., Hristov, V., Keating, B., Kim, M. G., Lee, D. H., Levenson, L. R., Mason, P., Matsumoto, T., Matsuura, S., Nam, U. W., Renbarger, T., Sullivan, I., Suzuki, K., Tsumura, K., and Wada, T., "The Cosmic Infrared Background ExpeRiment (CIBER): A sounding rocket payload to study the near infrared extragalactic background light," *The Astrophysical Journal Supplement Series* **207** (Aug 2013).

[2] Bock, J., Sullivan, I., Arai, T., Battle, J., Cooray, A., Hristov, V., Keating, B., Kim, M. G., Lam, A. C., Lee, D. H., Levenson, L. R., Mason, P., Matsumoto, T., Matsuura, S., Mitchell-Wynne, K., Nam, U. W., Renbarger, T., Smidt, J., Suzuki, K., Tsumura, K., Wada, T., and Zemcov, M., "The Cosmic Infrared Background ExpeRiment (CIBER): The wide-field imagers," *The Astrophysical Journal Supplement Series* **207** (Aug 2013).

[3] Tsumura, K., Arai, T., Battle, J., Bock, J., Brown, S., Cooray, A., Hristov, V., Keating, B., Kim, M. G., Lee, D. H., Levenson, L. R., Lykke, K., Mason, P., Matsumoto, T., Matsuura, S., Murata, K., Nam, U. W., Renbarger, T., Smith, A., Sullivan, I., Suzuki, K., Wada, T., and Zemcov, M., "The cosmic infrared background experiment (ciber): The low resolution spectrometer," *The Astrophysical Journal Supplement Series* **207**, 33 (Aug 2013).

[4] Korngut, P. M., Renbarger, T., Arai, T., Battle, J., Bock, J., Brown, S. W., Cooray, A., Hristov, V., Keating, B., Kim, M. G., Lanz, A., Lee, D. H., Levenson, L. R., Lykke, K. R., Mason, P., Matsumoto, T., Matsuura, S., Nam, U. W., Shultz, B., Smith, A. W., Sullivan, I., Tsumura, K., Wada, T., and Zemcov, M., "The cosmic infrared background experiment (ciber): The narrow-band spectrometer," *The Astrophysical Journal Supplement Series* **207**, 34 (Aug 2013).

[5] Zemcov, M., Smidt, J., Arai, T., Bock, J., Cooray, A., Gong, Y., Kim, M. G., Korngut, P. M., Lam, A. C., Lee, D. H., Matsumoto, T., Matsuura, S., Nam, U. W., Roudier, G., Tsumura, K., and Wada, T., "Origin of near-infrared extragalactic background light anisotropy," *Science* **346**, 732–735 (nov 2014).

[6] Cooray, A., Smidt, J., De Bernardis, F., Gong, Y., Stern, D., Ashby, M. L. N., Eisenhardt, P. R., Frazer, C. C., Gonzalez, A. H., Kochanek, C. S., Kozłowski, S., and Wright, E. L., "Near-infrared background anisotropies from diffuse intrahalo light of galaxies," *Nature* **494**, 514–517 (October 2012).

[7] Santos, M. R., Bromm, V., and Kamionkowski, M., "The contribution of the first stars to the cosmic infrared background," *Monthly Notice of the Royal Astronomical Society* **336**, 1082–1092 (November 2002).

[8] Kashlinsky, A., Arendt, R., Gardner, J. P., Mather, J. C., and Moseley, S. H., "Detecting population III stars through observations of near-infrared cosmic infrared background anisotropies," *The Astrophysical Journal* **608**, 1–9 (June 2004).

[9] Kashlinsky, A., Arendt, R. G., Mather, J., and Moseley, S. H., "New measurements of cosmic infrared background fluctuations from early epochs," *The Astrophysical Journal* **654**, L5–L8 (January 2007).

[10] Kashlinsky, A., Arendt, R. G., Ashby, M. L. N., Fazio, G. G., Mather, J., and Moseley, S. H., "New measurements of the cosmic infrared background fluctuations in deep Spitzer/IRAC survey data and their cosmological implications," *The Astrophysical Journal* **753** (July 2012).

[11] Cooray, A., Gong, Y., Smidt, J., and Santos, M. R., "The near-infrared background intensity and anisotropies during the epoch of reionization," *The Astrophysical Journal* **756** (September 2012).

[12] Lanz, A., Arai, T., Battle, J., Bock, J., Cooray, A., Hristov, V., Korngut, P., Lee, D.-H., Mason, P., Matsumoto, T., Matsuura, S., Morford, T., Onishi, Y., Shirahata, M., Tsumura, K., Wada, T., and Zemcov, M., "Studying extragalactic background fluctuations with the cosmic infrared background experiment 2 (ciber-2)," *Proc. SPIE* **9143** (2014).

[13] Matsumoto, T., Seo, H. J., Jeong, W.-S., Lee, H. M., Matsuura, S., Matsuhara, H., Oyabu, S., Pyo, J., and Wada, T., "Akari observation of the fluctuation of the near-infrared background," *The Astrophysical Journal* **742**, 124 (dec 2011).

[14] Cooray, A., Smidt, J., de Bernardis, F., Gong, Y., Stern, D., Ashby, M. L. N., Eisenhardt, P. R., Frazer, C. C., Gonzalez, A. H., Kochanek, C. S., Kozłowski, S., and Wright, E. L., "Near-infrared background anisotropies from diffuse intrahalo light of galaxies," *Nature* **490**, 514–516 (oct 2012).

[15] Kashlinsky, A., Arendt, R. G., Ashby, M. L. N., Fazio, G. G., Mather, J., and Moseley, S. H., "New measurements of the cosmic infrared background fluctuations in deep spitzer/irac survey data and their cosmological implications," *The Astrophysical Journal* **753**, 63 (jul 2012).

[16] Tsumura, K., Matsumoto, T., Matsuura, S., Sakon, I., Tanaka, M., and Wada, T., "Low-resolution spectrum of the diffuse galactic light and 3.3 μm pah emission with the akari infrared camera," *Publications of the Astronomical Society of Japan* **65**, 120 (December 2013).

[17] Tsumura, K., Matsumoto, T., Matsuura, S., Pyo, J., Sakon, I., and Wada, T., "Low-resolution spectrum of the zodiacal light with the akari infrared camera," *Publications of the Astronomical Society of Japan* **65**, 119 (December 2013).

[18] Pyo, J., Matsumoto, T., Jeong, W.-S., and Matsuura, S., "Brightness and fluctuation of the mid-infrared sky from akari observations toward the north ecliptic pole," *The Astrophysical Journal* **760**, 102 (December 2012).

[19] NASA Sounding Rockets Program Office, *The NASA Sounding Rocket Program Handbook*.

[20] Tsumura, K., Battle, J., Bock, J., Cooray, A., Hristov, V., Keating, B., Lee, D. H., Levenson, L. R., Mason, P., Matsumoto, T., Matsuura, S., Nam, U. W., Renbarger, T., Sullivan, I., Suzuki, K., Wada, T., and Zemcov, M., "Observations of the near-infrared spectrum of the Zodiacal Light with CIBER," *The Astrophysical Journal* **719**, 394–402 (August 2010).

[21] Arai, T., Matsuura, S., Bock, J., Cooray, A., Kim, M. G., Lanz, A., Lee, D. H., Lee, H. M., Sano, K., Smidt, J., Matsumoto, T., Nakagawa, T., Onishi, Y., Korngut, P., Shirahata, M., Tsumura, K., and Zemcov, M., "Measurements of the mean diffuse galactic light spectrum in the 0.95-1.65 m band from ciber," *The Astrophysical Journal* **806**, 69 (jun 2015).

[22] James, W. B., Richard, B., David, G., Donald, L., Markus, L., Eric, C. P., Thomas, S., William, E. T., Majid, Z., and Joseph, Z., "Teledyne imaging sensors: Infrared imaging technologies for astronomy & civil space," *Proc. SPIE* **7021** (2008).

[23] Moseley, S. H., Arendt, R. G., Fixsen, D. J., Lindler, D., Loose, M., and Rauscher, B. J., "Reducing the read noise of H2RG detector arrays: eliminating correlated noise with efficient use of reference signals," *Proc. SPIE* **7742** (2010).